Journal of Energy Storage 68 (2023) 107587

Contents lists available at ScienceDirect

Journal of Energy Storage

journal homepage: www.elsevier.com/locate/est

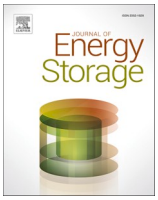

Research papers

Optimized Ca-looping thermochemical energy storage under dynamic operation for concentrated solar power

S. Pascual, L.M. Romeo *, P. Lisbona

Departamento de Ingeniería Mecánica, Escuela de Ingeniería y Arquitectura, Edificio Betancourt, María de Luna s/n, Universidad de Zaragoza, 50018, Spain

ARTICLE INFO

Keywords:
Calcium-looping
Thermochemical energy storage
Concentrated solar power
Daily operational performance

ABSTRACT

The massive deployment of renewable energy sources and carbon capture technologies are required to achieve net zero emissions target by 2050. Calcium Looping (CaL) is a promising Thermochemical Energy Storage (TCES) system which improves the dispatchability of Concentrating Solar Power (CSP) plants. CaL TCES configurations found in literature focus on a steady-state analysis of thermal-to-electric efficiency of the CSP plants. In this work, the operation of the CaL TCES system for a CSP plant is economically optimized taking into account the seasonal and daily variations of solar resource and electricity prices. The defined methodology determines the operating performance of the CaL TCES which maximize the economic incomes of the CSP and the daily profiles of energy production and storage for representative days of the different seasons/periods of the year. Results show that it is possible to obtain good economic results and operate the CSP + storage for a daily maximization of incomes. Obtained results are also useful for the final design of the system and for the definition of the size required for the storage equipment.

1. Introduction

The Calcium Looping (CaL) technology was developed in the last decades as a capture system for carbon intensive sectors, such as fossil-fuel based power plants [1] or cement plants [2]. More recent research works assess CaL carbon capture associated to bioenergy production from wastes [3] or renewable sources as biomass [4] to achieve zero or negative emissions. However, Barker proposed the CaL process for the first time in 1974 as a potential Thermochemical Energy Storage (TCES) [5]. This interest has been reactivated in the last decade to be coupled with renewable energy sources. The roadmap reported by the International Energy Agency (IEA) to achieve net zero emissions by 2050 includes (i) the increase of energy storage to support energy production and (ii) the importance of implementing low-carbon power plants [6]. Thus, the CaL system will play a crucial role in both (i) the decarbonization of the energy and industrial sectors and (ii) the improving the capacity factor of renewable power plants.

The CaL process is based in the cyclic calcination/carbonation reversible reaction of limestone. The limestone ($CaCO_3$) is an Earth-abundant, cheap and non-toxic sorbent material of CO_2 [7,8]. The endothermic calcination reaction of $CaCO_3$ form calcium oxide (CaO) and CO_2 (Eq. (1)). The exothermic carbonation reaction occurs when CaO partially reacts with CO_2 to form $CaCO_3$ (reverse Eq. (1)), releasing thermal energy. After the carbonation step, a mixture of partially carbonated solids is found where CaO and $CaCO_3$ coexist in the same particle. The carbonation degree will depend on the operating conditions of the CaL process which are different for CO_2 capture or TCES applications.

$$CaCO_{3\,(s)} \leftrightarrows CaO_{(s)} + CO_{2\,(g)} \Delta H_R^{\circ} = +178\ kJ/mol \quad (1)$$

Under carbon capture process, the concentration of CO_2 is 10–15 % *v*/v during carbonation reaction at 650 °C [9]. The energy demanded by calcination reaction is usually supplied by oxy-fuel combustion at 950 °C, achieving a high CO_2 concentration during calcination [10]. Regarding TCES, the reactors atmosphere may reach 100 % CO_2 at 950 °C and 850 °C, for calciner and carbonator respectively [11,12]. High operating temperatures of CaL TCES system cause a decay of sorbent capacity with the number of carbonation/calcination cycles [13,14]. Loss of porosity and pore plugging takes place, inducing thermal and chemical sintering [15–18]. The loss of sorbent reactivity is one of the main issues to be solved. The sorbent deactivation has been extensively investigated under carbon capture conditions, developing well-fitted carbonation models [9,19,20]. Under TCES conditions, further experimentation is required to develop robust sorbent

* Corresponding author.
E-mail address: luismi@unizar.es (L.M. Romeo).

https://doi.org/10.1016/j.est.2023.107587
Received 24 January 2023; Received in revised form 10 April 2023; Accepted 29 April 2023
Available online 19 May 2023
2352-152X/© 2023 The Authors. Published by Elsevier Ltd. This is an open access article under the CC BY license (http://creativecommons.org/licenses/by/4.0/).

deactivation models. Several proposals have been addressed in literature to limit the CaO activity decay for CO_2 capture: (i) mechanical [21,22], thermal [23] or steam-enhanced [24] limestone pretreatments [25], (ii) use of ZrO_2 [26,27] or Al_2O_3 [27,28] as inert stabilizers in sorbent doping. Regarding sorbents subjected to TCES conditions, the most developed techniques to improve sorbent conversion are based on: (i) limestone pretreatments, such as thermal [29] or steam [30,31], (ii) sorbent doping [32,33], even with eutectic alkali chloride salts [34] or ZrO_2 [35] as inert promoter [36], (iii) natural limestone enhancement [17], or (iv) synthetic Ca-based sorbents development [37], even adding dark inert substances to improve solar energy absorption [32,38,39]. Moreover, calciner and carbonator reactors can be pressurized to minimize the deactivation of the sorbent due to sintering at high operating temperatures. A low-pressure calcination operation (0.01 bar) was proposed by Ortiz et al. to mitigate sintering issues under calcination and loss of sorbent capacity during carbonation step [40]. The CaL process can be easily thermally integrated as TCES in Concentrating Solar Power (CSP) plants, whose operating temperature is above 800 °C [41,42]. Since the $CaCO_3$ energy density is up to 490 kWh/t [43], the storage capacity of the CaL process will be higher than sensible and latent thermal energy storage systems, minimizing energy losses of seasonal storage. Furthermore, a recent research states a lower environmental impact of the CaL-TCES system compared to molten salts energy storage integrated into CSP, being 40 % lower in CO_2 equivalent emissions [44].

Previous research investigated the integration of different power cycles in CSP plants with CaL TCES. The future next generation of CSP facilities should be coupled with high-efficient power blocks to enhance their energy and economic feasibility, such as Brayton [45]. Thus, more efficient power cycles are currently being developed to take advantage of the high temperature solar energy recovery potential at carbonation stage of the CaL TCES system [46]. Tesio et al. compares the integration of two Brayton cycles in a CaL TCES system (supercritical CO_2 and helium), resulting supercritical CO_2 Brayton cycle the cheapest option and the helium Brayton cycle the most efficient alternative [39]. Nevertheless, the most suitable power cycle for actual ongoing applications is the steam Rankine cycle [47]. In general, these works analyze the system under stationary operation. However, the variability of solar resource lead to a dynamic operation of the CaL TCES that strongly influences the design and size of the plant equipment as it has been demonstrated elsewhere [48]. More recent investigations of the CaL TCES system integrated in CSP plants is focused on the plant capacity factor improvement, minimizing the facility investment cost. The dispatch enhancement is provided through (i) the combination of solar power technologies, CSP and photovoltaic (PV) plants [49,50], (ii) the oversizing the solar field [51] and (iii) the integration of CSP with combined cycle plants [40,52,53]. The hybridization between solar power technologies (CSP and PV) is proposed by Bravo et al., reaching up to 73 % capacity factor [50]. Under solar energy availability, energy demand is supplied by CSP and PV technologies. The energy stored by the CaL TCES system during the day is recovered when solar power technologies are shut down [49,50]. An operational multi-objective optimization is applied to maximize the produced net power per year with the minimum financial and energy cost, being the input variables the hourly solar power availability, the minimum energy demand and economic data. The optimum technical and economic performance and the hourly energy demand are the result of the multi-objective operational methodology, achieving an overall efficiency of 33.8 % [49]. Secondly, the solar field oversizing is investigated by Tregambi et al. to store the recovered energy at night when solar energy is available, considering an steady state operation with 12.1 h of sunlight [51]. The most recent integration of CSP with combined power block is proposed by Ortiz et al. to improve the plant capacity factor [53]. Under sunlight hours, the CSP plant provides thermal energy to the CaL TCES system to store energy and to the combined power cycle to supply energy demand. When solar energy is unavailable, the stored energy is recovered to supply energy demand [52]. The applied operational methodology is based on recovering the energy stored within sunlight hours at a constant rate during the night. The hourly energy demand is shown as a result within four selected days with different solar radiation, achieving an overall efficiency of 45 % [53]. Moreover, Ortiz et al. assess the CaL TCES system operation under a recent proposal based on low-pressure calcination within the integration of CSP and combined power blocks [40]. The CaL TCES operation is analyzed within typical spring and summer days, obtaining the daily pattern of demanded energy, stored energy and efficiency (above 30 %). The energy stored during solar energy availability is proportionally recovered at night [40], as in most of the previous research. Since the solar resource varies hourly, daily and seasonally, most of the research found in literature assesses typical days/months or the year as a whole to optimize design and minimize the required size of the plant equipment and its corresponding investment cost. In these works, the energy stored during sunlight hours is proportionally retrieved during the night or when solar power is unavailable, dismissing energy demand patterns to set the best operating strategies.

As highlighted, there is a gap in the analysis of dynamic operation of the CaL TCES along the day. This work contributes to the study of transient operation when applying CaL TCES to CSP and both, the solar energy available and the hourly electricity price varies depending on the season of the year and the hour of the day. Therefore, the novelty of this work relies in the definition of the methodology to decide the operation points of the CaL TCES system along the day/year while optimizing the economic revenue of the associated CSP plant without power supply backup. The CaL TCES configuration proposed in the present study does not contemplate the oversizing of either the storage tanks or the solar field. The energy storage is designed to balance the solar energy availability with the energy demand variability, maximizing the economic and energy performance of the CaL TCES system. The novel operating methodology proposal could be able to define a realistic operational pattern of the CaL TCES system integrated into CSP plants. Besides, an ideal threshold scenario of total separation of carbonated solids scenario is considered in this study [54,55], minimizing the energy penalty associated to the circulation of a large inert solid material [56] due to the low carbonation activity [57] and the plant size and investment cost.

The aim of the present study is to define a systematic methodology to maximize the daily incomes derived from electricity production of the CSP plant associated to the CaL TCES. Besides, adequate criteria are defined to select the representative days to apply the operating methodology, considering days of minimum and maximum daily average solar irradiation and daily electricity prices. The assessment of the CaL TCES system operation with the established methodology provides the estimation of: (i) the daily thermal energy production profile and its corresponding incomes from electricity sales; (ii) the daily storage evolution of the gas and solids; and (iii) the daily operating pattern maximizing the efficiency of the system.

2. CaL TCES system description

The Calcium-Looping thermochemical energy storage system under study is illustrated in Fig. 1, and described in detail [55].

An ideal scenario of total separation of solids after carbonation step is assessed in this study leading to the minimization of energy penalty associated to solids management. The main equipment involved in the CaL TCES system are: (i) Calciner and Carbonator reactors, (ii) Solids Separation Unit (SSU), (iii) Storage Tanks of CO_2 (ST3), CaO (ST2) and $CaCO_3$ (ST1) and (iv) Heat Exchangers (HE).

2.1. Selected location and solar resource

To illustrate the methodology with an example, a location has been selected for this study, the PS10 solar thermal power plant (37.443°N, 6.25°W) at Seville (Spain). The component of solar irradiation captured by heliostats is the Direct Normal Irradiation (DNI) [50], extracted for a

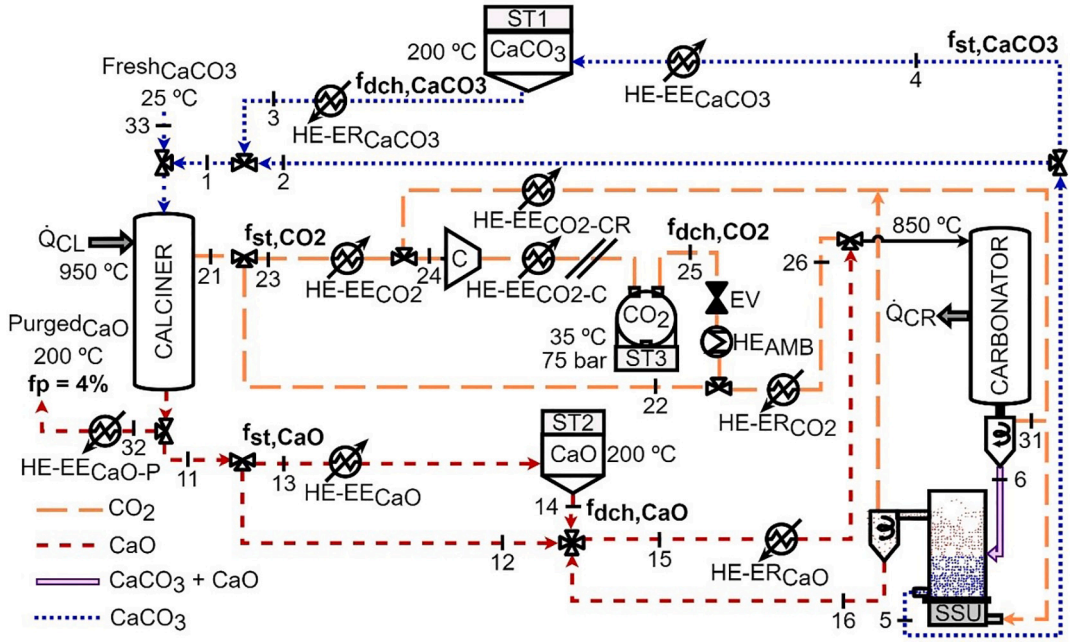

Fig. 1. Conceptual scheme of the CaL TCES system under study.

Typical Meteorological Year (TMY) from the Photovoltaic Geographical Information System (PVGIS) tool of European Commission [58]. The DNI data from a TMY with hourly time-steps and the solar field design provide the hourly solar power supplied to the CSP plant throughout a year. The hourly solar power reaches the calciner, $\dot{Q}_{SOLAR}(h)$, and this power is determined through Eq. (2), using the hourly Direct Normal Irradiation (DNI in MW/m^2), the annual optical efficiency of the solar field ($\eta_{opt,y}$), the annual thermal efficiency of the solar receiver ($\eta_{ther,y}$) and the Solar Field Area (SFA in m^2).

$$\dot{Q}_{SOLAR}(h) = DNI(h) \bullet \eta_{opt,y} \bullet \eta_{ther,y} \bullet SFA \quad (2)$$

A reasonable solar field area of 290,482 m^2 is assumed with an annual optical efficiency ($\eta_{opt,y}$) of 64.7 % and an annual thermal efficiency ($\eta_{ther,y}$) of 92.8 %. The optical and thermal efficiencies values correspond to the annual performances of the solar field of the PS10 solar power plant [59].

2.2. Calciner

The calciner, located inside the solar receiver, operates at 950 °C under pure CO_2 atmosphere at 1 bar to ensure the complete decomposition of $CaCO_3$ into CaO and CO_2 [60]. The selection of the calciner nominal size ($\dot{Q}_{CL,nom}$) must maximize the solar thermal energy input for the selected location. The Load Duration Curve considering the provided solar irradiation data and solar field design is represented in Fig. 2 where the black curve represents the hourly solar power, $\dot{Q}_{SOLAR}$, versus the number of operation hours per year in which this power is available.

The optimal calciner size is obtained through the maximization of the grey area in Fig. 2, that represent the energy available for the calciner (the product of power available and number of hours). The maximum solar thermal energy supplied to calciner at nominal load ($E_{CL,nom}$ = 222.6 GWh). The nominal calciner power, $\dot{Q}_{CL,nom}$, equals the solar power which provides this largest amount of energy, $\dot{Q}_{SOLAR}$ (h_{nom}) where h_{nom} represents the sunlight hours at nominal load for such calciner size, satisfying the condition given in the Eq. (3):

$$E_{CL,nom}(h_{nom}) = max\{E_{CL}(h)\,|h \in \mathbb{R}, h > 0\} \quad (3)$$

The obtained calciner nominal size ($\dot{Q}_{CL,nom}$) is 100MWth and a

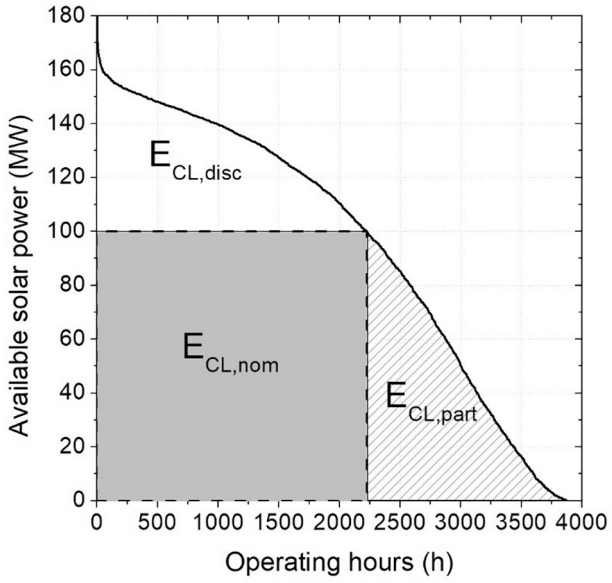

Fig. 2. Load duration curve: the shaded areas represent the thermal energy received in the calciner at full or partial load.

calciner of such size can operate at nominal load during 2226 h per year in the selected location. Besides, the calciner can operate at partial loads, supplying the thermal energy represented by the stripped area ($E_{CL,part}$ = 78.3 GWh). The discarded surplus solar energy ($E_{CL,disc}$ = 76.8 GWh) is the solar resource not used above the calciner nominal load.

The heat received into the calciner ($\dot{Q}_{CL}$) is fully used to heat up the inlet stream to 950 °C and provide the required heat to the calcination step. The calciner inlet streams include (i) the fresh limestone (stream 33) and (ii) the $CaCO_3$ diverted from the Solids Separation Unit (SSU) or the Storage Tank ST1. The fresh limestone (stream 33) counterbalances the purged CaO (stream 32) fed into the system to avoid a quick deactivation of the sorbent with the number of calcination/carbonation cycles and to keep a reasonable average sorption activity of the solid

population in the carbonator. The sorbent purge (f_p) is given as a fraction of the CaO molar flow produced in calcination reaction. The CaO (stream 1) and CO_2 (stream 21), produced in the calciner, can be directed to the carbonator or to their corresponding Storage Tanks (ST2 and ST3), according to the carbonator energy demand.

2.3. Carbonator

The carbonator operation pressure is slightly above the atmospheric pressure (1.2 bar) to facilitate the solids circulation between calciner and carbonator [61]. The exothermic carbonation reaction occurs at 850 °C under pure CO_2 atmosphere. As in CO_2 capture applications, there is a decay in sorbent conversion and the average sorption activity of the population of particles circulating in the system has been calculated through Eq. (4) where X_N is estimated using the carbonation decay model of Valverde et al., Eq. (5) [19,20], adjusted to experimental data obtained at calcination/carbonation conditions for this application [54]. The experimental carbonation tests were performed in a Fluidized Bed (FB) considering 850 °C for carbonation and 950 °C for calcination, both under pure CO_2 atmosphere and *Sardo* limestone as sorbent [54].

$$X_{ave} = \sum_{1}^{\infty} r_N \bullet X_N \tag{4}$$

$$X_N = \frac{X_1}{\frac{1}{1-\frac{X_r}{X_1}} + k \bullet (N-1)} + X_r \tag{5}$$

The parameters (k, X_r and X_1) were determined using a least squares regression and the best fit curve is represented in Fig. 3a. After 20 cycles, the conversion drops to 0.088, considering a deactivation constant (k) of 1.10 and a residual conversion (X_r) of 0.06. Once the CaO average sorption capacity is calculated (X_{ave}), the CO_2 capture efficiency can be determined through Eq. (6) using the Ca/C molar ratio (R) introduced into the carbonator.

$$\eta_{capt} = X_{ave} \cdot R \tag{6}$$

The value of R is imposed when the nominal power in the calciner ($\dot{Q}_{CL,nom}$), the CaO purge fraction (f_p) and the storage and discharge flowrates of CaO and CO_2 are defined. A sensitive analysis of the spent material purge flowrate was carried out to assess the behavior of both parameters and select an adequate purge, Fig. 3b.

Large Ca/C molar ratios (R) improve the carbon capture efficiency but in carbon capture systems also increase the cost of the system due to a more intensive solid circulation [62]. In literature it has been proposed to combine CSP with cement industry to reduce costs [63]. Besides, lab-scale facilities for carbon capture in the range of 10–75 kWth have reported successful operation of the process with calcium looping ratios between 7 and 18, whose power is close to industrial scale [64,65]. Therefore, a value of CaO purge (f_p) of 4 % corresponding to a Ca/C molar ratio (R) of 7.28 and an average sorption capacity of 13.21 % has been chosen to obtain a carbon capture efficiency above 90 %. Under the selected operating conditions, the maximum power released from the carbonator achieves 88 MWth.

2.4. Operation of the system

The CaL TCES system operates within two modes: energy storage and energy release. When the system works in Energy Storage Operation Mode (ESOM), the calciner load is higher than the carbonator load. Therefore, the CaO and CO_2 from calciner are partially stored and limestone from Storage Tank ST1 must be discharged to supply the amount of $CaCO_3$ required for the calcination reaction. Whenever the system operates under Energy Retrieval Operation Mode (EROM), the calciner load is lower than the carbonator load. Thus, the discharge of CaO particles and CO_2 from the Storage Tanks ST2 and ST3 to the carbonator is required. In the same way, the $CaCO_3$ from the SSU must be partially stored since the available solar resource (calciner load) is not enough to calcine the total amount of limestone formed in the carbonator.

A given operating point is completely defined by the pair of calciner and carbonator loads and the storage/discharge fractions of CaO or $CaCO_3$. There exist many possible combinations of storage/discharge fractions which lead to a specific pair of calciner/carbonator loads. However, not all of these operation points are considered technically feasible and an operation map of the facility has been constructed [55] meeting four criteria:

- C.1. The heat exchangers HE-EE, Fig. 1, must always release thermal energy with heat losses of 2 % of the exchanged power. However, the heat exchangers HE-ER must always require a thermal energy supply.
- C.2. Under ESOM, no storage of $CaCO_3$ is allowed. Whereas under EROM, the CaO and CO_2 streams from calciner are not stored but fully directed to carbonator.
- C.3. Regarding size equipment and whenever possible, a minimum partial load of 50 % (carbonator, HE-EE-CO2, HE-EE-CaO and HE-

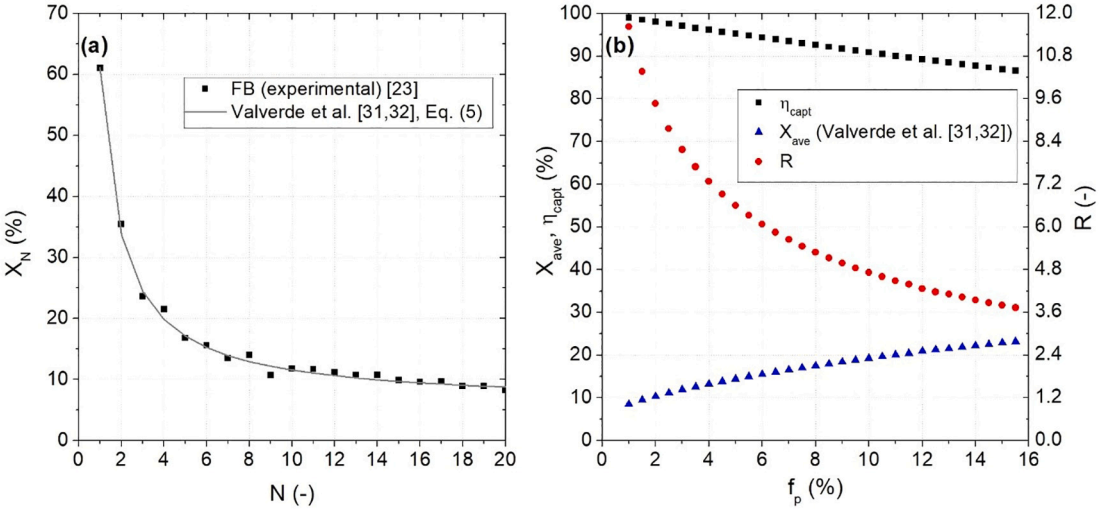

Fig. 3. (a): Best fit curve from Eq. (5) to experimental data under FB conditions. (b): Sorbent average activity and Ca/C molar ratio under 100 MW_{th} calciner power for different purges.

EE-CaCO3) and a maximum energy demand of 50 % (HE-ER-CaCO3) are established for equipment with high nominal power. However, the full energy storage mode is also contemplated.

- C.4. The selection of a single operating point for each pair of calciner/carbonator loads, among those technically possible ones, must maximize the efficiency of energy availability (η_{av}) for EROM and energy storage efficiency (η_{st}) for ESOM [55].

3. Methodology

The proposed methodology includes (i) the selection of representative days within a standard year in a specific location, which depends on solar resource (DNI) and Electricity Prices (EP) as variable inputs and (i) the formal economic optimization under several constraints to maximize the daily incomes for a specific case study, being influenced by the recovered energy from the CaL TCES system. The constraints of the dynamic operating methodology are focused on the maximization of energy performance and the daily net balance of the stored energy without backup energy supply. The defined operational methodology is coded and implemented by a genetic method included in the Engineering Equation Solver (EES) software [66]. The daily patterns of stored and recovered energy and the operation of the CaL TCES system are the result of the novel operating methodology based on solar power and energy demand variability.

3.1. Selection of representative days

The novel dynamic operating methodology is able to manage variable inputs from any specific location. The operating model inputs are the solar radiation in a specific location and the electricity price governed by the country energy market in which the CSP facility is located. A case study is analyzed to extract quantitative results from the operation methodology application in a specific location with defined profiles of solar radiation (DNI) and energy demand (EP). Eight representative days which cover different potential conditions throughout the year are selected to validate the operation pattern of the CaL TCES system derived from the proposed methodology. The selected days cover maximum and minimum of DNI and EP for different seasons of the year, whose description is shown in Fig. 4.

The daily solar resource input is extracted from PVGIS tool [58] at the Spanish province of Seville, as described in Section 2.1. The maximum and minimum daily average DNI are found during summer and winter time. The minimum daily average EP usually corresponds to spring or autumn days. The electricity prices data are extracted for a standard year (pre-war and pre-pandemic) from Spanish electrical grid (Red Eléctrica Española - REE) [67], which have been collected for each hour throughout the year 2019.

Regarding the solar radiation along the representative days, two restrictions have been assumed. The average number of sunlight hours of the location selected (Seville) ranges between 9 and 14 h according to Spanish Geographic Institute (IGN) [68]. Besides, the representative days must allow a continuous supply of energy to the solar receiver during the sunlight hours. Very cloudy extreme days are discarded. Once the representative days are selected, the hourly EP and DNI data are extracted from the databases. The electricity price and solar radiation pattern under each representative day selected are defined in Table 1.

The spring and autumn minimum daily average EP representative days ($SP_{EP,min}$ and $AU_{EP,min}$) have an EP profile with significant gap between the minimum and maximum hourly EP ($EP_{max} - EP_{min}$) of 41.36 €/MWh and 33.76 €/MWh, respectively. While under the spring and autumn maximum daily average EP representative days ($SP_{EP,max}$ and $AU_{EP,max}$), the EP profile is uniform without sharp variations along the day. The days selected within spring have similar solar radiation (7626.91 and 8564.28 MWh per day for $SP_{EP,min}$ and $SP_{EP,max}$, respectively). In the same way, the autumn representative days present a daily average solar radiation between 202 and 270 MWh.

The summer and winter minimum average DNI representative days ($SU_{DNI,min}$ and $WI_{DNI,min}$) have the second and first lowest total solar radiation (4448.56 MWh and 1216.30 MWh) within the selected days,

Table 1
Main characteristic values of the daily input variables (EP and DNI) under the representative days.

Representative days		Electricity price (EP)		Direct Normal Irradiation (DNI)	
		$EP_{d,ave}$	Gap[a]	$DNI_{d,ave}$	$DNI_{d,total}$
		(€/MWh)		(MWh)	
Spring	$SP_{EP,min}$	29.69	41.36	317.79	7626.91
	$SP_{EP,max}$	58.43	5.47	356.85	8564.28
Autumn	$AU_{EP,min}$	18.88	33.76	202.17	4852.02
	$AU_{EP,max}$	57.84	19.65	269.46	6467.13
Summer	$SU_{DNI,min}$	36.29	15.22	185.36	4448.56
	$SU_{DNI,max}$	50.95	11.5	437.85	10,508.29
Winter	$WI_{DNI,min}$	32.72	28.28	50.68	1216.30
	$WI_{DNI,max}$	48.77	17.5	339.15	8139.67

[a] Range between maximum and minimum hourly Electricity Price ($EP_{max} - EP_{min}$).

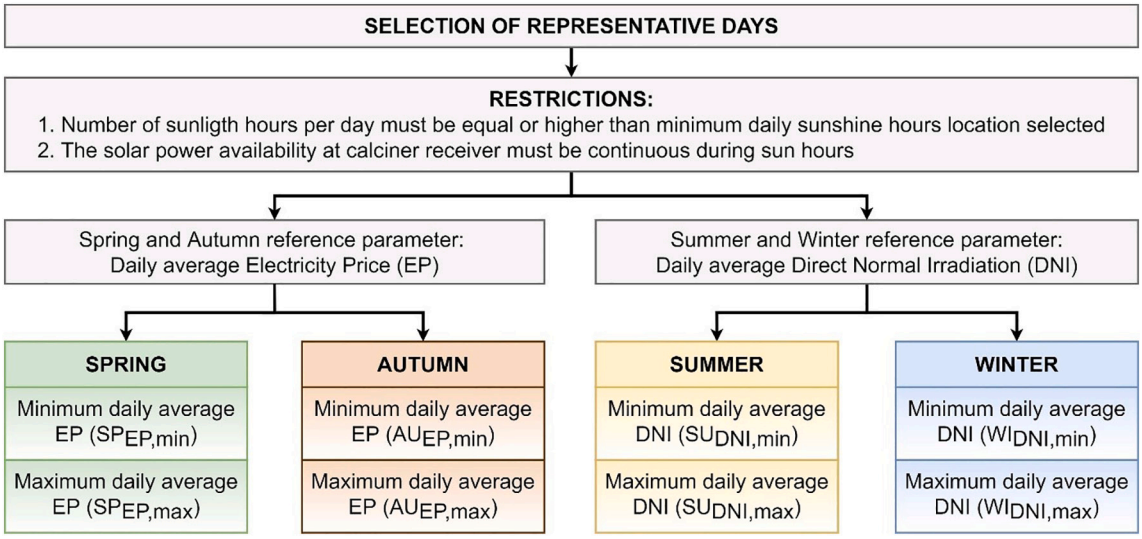

Fig. 4. Criteria for the selection of representative days.

respectively. The summer maximum daily average DNI ($SU_{DNI,max}$) is the representative with the highest daily average solar radiation (437.85 MWh). While the winter maximum daily average DNI representative day ($WI_{DNI,max}$) profile similar to the days selected within spring season. The EP profile is smoother during $SU_{DNI,min}$, $SU_{DNI,max}$ and $WI_{DNI,max}$ representative days with a gap of 15.22, 11.50 and 17.50 €/MWh between minimum and maximum hourly EP, respectively, than along $WI_{DNI,min}$ representative day (28.28 €/MWh).

The hourly DNI data within each representative day is used to determine the hourly available solar heat power ($\dot{Q}_{SOLAR}$), applying Eq. (2). The solar power invested in the calcination reaction ($\dot{Q}_{CL}$) represents the power supplied to calciner receiver, discarding the surplus of solar power above the nominal calciner power ($\dot{Q}_{CL,DISC}$).

3.2. Economic operating methodology

The economic methodology applied to maximize the daily incomes is illustrated in Fig. 5. After gathering the input variables of the specific case study (DNI and EP), the novel dynamic operating methodology is assessed under each selected day. The dynamic operation methodology aims to maximize daily financial income, which is directly related to the recovered energy from carbonator to supply the energy demand. Input data include the daily EP profile and the available solar power in the calciner, as described in blue area of Fig. 5. The available solar energy is determined from the DNI of the specific location for each day and the daily EP profile corresponds to the assessed day. Grey area of Fig. 5 represents the core of the operating model. Constraints related to the net balance of the daily stored energy and the CaL TCES operation are assumed. A constant storage level is kept at the beginning and end of the day ($E_{st,BoD} = E_{st,EoD}$). The second constraint forces the CaL TCES system to only operate at points that maximize energy efficiency within the operation map, meeting the criteria described in Section 2.4. A genetic method incorporated in the EES software is applied to maximize the daily income (In_d) as target variable per each representative day. Besides the incorporation of the input data per each representative day and the constraints to the EES software, the maximization algorithm requires to set the lower and upper bounds of independent variables and three internal parameters. The independent variables are the carbonator load (L_{CR}) for all the hours per day, given the relationship between the target

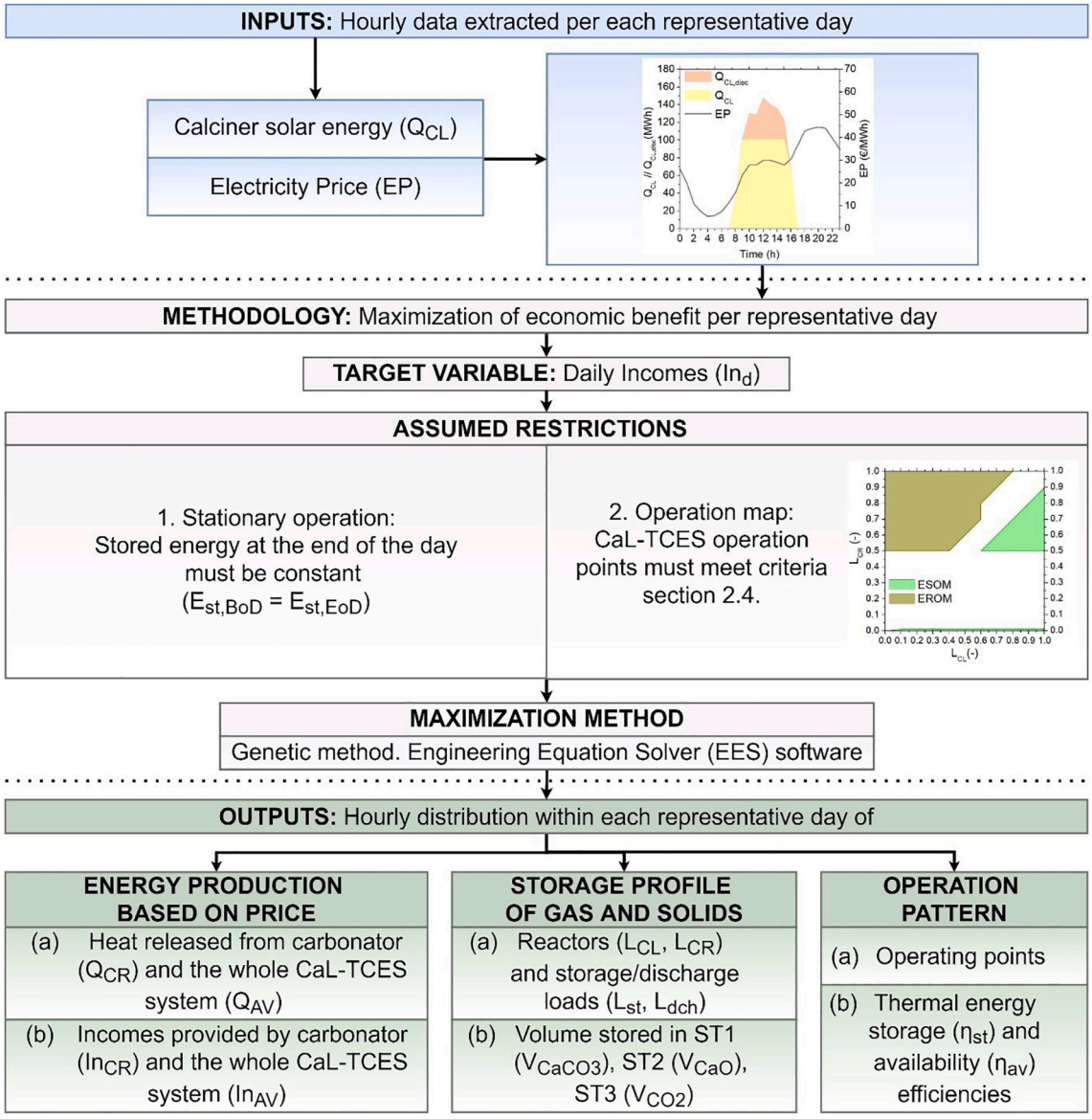

Fig. 5. Daily incomes maximization methodology flowchart. (For interpretation of the references to color in this figure legend, the reader is referred to the web version of this article.)

variable and the energy recovered from the carbonator. The three internal parameters must be set to their maximum value to reach the greatest robustness in the optimization calculations. As a result of the dynamic operation model (see green area of Fig. 5), the daily profiles of recovered and stored energy are obtained, as well as the operational map of each selected day that maximizes the economic and energy efficiency of the CaL TCES system.

The objective function pretends to maximize the daily incomes (In_d), calculated as the sum of the product of the electric power retrieval and the EP for all the hours of the day. Two possibilities have been considered. The first one is only related to the heat released in the carbonator (Eq. (7)) and the second one to the heat released in the carbonator together with the rest of available heat from the heat exchangers (Eq. (8)).

$$In_{CR,h} = \frac{\dot{Q}_{CR,h}}{\dot{Q}_{CR,nom}} \bullet \eta_{SRPC} \bullet EP_h; \text{being } In_d = \sum_{h=0}^{23} In_{CR,h} \quad (7)$$

$$In_{AV,h} = \frac{\dot{Q}_{CR,h} + \sum \dot{Q}_{HE\ EE,h}}{\dot{Q}_{CR,nom}} \bullet \eta_{SRPC} \bullet EP_h; \text{being } In_d = \sum_{h=0}^{23} In_{AV,h} \quad (8)$$

The hourly incomes generated by carbonator thermal energy ($In_{CR,h}$) and the total available energy ($In_{AV,h}$) are presented in €/h per MW installed in the carbonator, considering a thermal performance of 35,55 % for a steam Rankine power cycle (η_{SRPC}) associated to the CaL TCES system [47]. For both income calculation expressions, the same thermal to electrical conversion was considered since the carbonator and heat exchangers named EE release heat at high temperature. The carbonator always releases thermal energy at 850 °C. The EE heat exchangers can release heat from 950 to 50 °C, with the greatest heat availability between 950 and 200 °C [55]. Thus, the high-temperature heat from the CaL TCES system can be well integrated into a steam cycle.

The main constraint applied to the daily incomes maximization problem is the daily conservation of the stored energy (constant amount of stored energy at the end and the beginning of the day). The selected optimization range is one day (24 h) although the methodology could be applied to a different timeframe. Evidently, the storage silos will accordingly increase their size when the considered period is higher. The second restriction focuses on the operating points under each pair of calciner/carbonator loads. The CaL TCES system must operate within the operating map, meeting the criteria of Section 2.4. Under any calciner load, the energy released from the carbonator rises when carbonator load increases. The maximization of daily incomes will be achieved when the carbonator is operated at full load during those hours with highest EP. Thus, there may be hours of the day when no energy is retrieved by the carbonator or the whole system is disconnected.

The EES software was used to maximize the target variable (In_d) through a genetic method [66]. The genetic algorithm is provided by the public domain Pikaia optimization program developed by Paul Charbonneau and Barry Knapp at National Center for Atmospheric Research (NCAR) [69]. The algorithm inputs are (i) the independent variables (L_{CR} for all hours of a day) and its bounds (from 0 to 1) and (ii) the values selected for the three parameters of the genetic method. The parameters in the genetic method are the number of individuals and generations and the maximum mutation rate, which allow to identify the optimum value for the maximizing variable. The higher the value assigned to the parameters of the genetic method, the greater the computational effort and the greater the robustness of the optimal result. For this work, the values set for the three parameters are their maximum possible values (256 individuals, 2048 generations and 0.7 the maximum mutation rate). Once the input variables and parameters value are set, the best solution for the maximization of the target variable will be found when the computing calculations finish.

As results, the operational loads of carbonator and calciner are obtained together with the daily storage profile. The volume stored of CO_2, (Eq. (9)) CaO (Eq. (10)) and $CaCO_3$ (Eq. (11)) is hourly obtained and the final design and sizing conditions of the CaL TCES system could be calculated.

$$V_{CO2,h} = \frac{\dot{m}_{st,CO2,h}}{\rho_{CO2\ (35°C,75bar)}} \quad (9)$$

$$V_{CaO,h} = \frac{\dot{m}_{st,CaO,h}}{\rho_{p,CaO} \bullet (1 - \varepsilon_{st})} \quad (10)$$

$$V_{CaCO3,h} = \frac{\dot{m}_{st,CaCO3,h}}{\rho_{p,CaCO3} \bullet (1 - \varepsilon_{st})} \quad (11)$$

The hourly stored volume of CO_2 ($V_{CO2,h}$) is calculated as the relation between the hourly amount of stored CO_2 ($\dot{m}_{st,CO2,h}$) and the CO_2 density at 35 °C and 75 bar conditions [55] ($\rho_{CO2\ (35°C,75bar)} = 273.71$ kg CO_2/m^3). The CaO and $CaCO_3$ hourly stored volume ($V_{CaO,h}$ and $V_{CaCO3,h}$) are calculated considering the effective particle densities of fresh material ($\rho_{p,CaO} = 1793$ kg CaO/m^3 and $\rho_{p,CaCO3} = 2930$ kg $CaCO_3$/m^3 [54]) with a void fraction (ε_{st}) of 0.30 in the Storage Tanks ST2 and ST1 [70]. The fresh material is assumed to occupy the maximum possible volume [54].

4. Results and discussion

Results include the determination of: (i) energy production, (ii) stored volume of gas and solids and (iii) operational pattern within the operation maps.

4.1. Daily distribution of energy production based on electricity price

Under each representative day, the hourly distribution of the energy production and the incomes derived from the heat generated by the CaL TCES system are determined. In the Appendix section the complete set of figures for the eight selected representative days can be consulted (see Figs. A.1, A.2, A.3 and A.4). The yellow area corresponds to the profile of the solar power available at calciner receiver ($\dot{Q}_{CL}$), whereas the orange area represents the surplus of solar energy which is discarded ($\dot{Q}_{CL,DISC}$). The dotted curve represents the energy released in the carbonator ($\dot{Q}_{CR}$) and the corresponding incomes (In_{CR}). While the dashed curve reports the energy released in the carbonator and heat exchangers named EE ($\dot{Q}_{AV}$) and the incomes related to the thermal energy available in the CaL TCES system (In_{AV}).

The thermal energy production (Fig. 6a) and the obtained incomes (Fig. 6b) for the representative day with the minimum daily average EP in spring ($SP_{EP,min}$) are illustrated in Fig. 6. During the hours with maximum EP (two peaks around 9 and 21 h), the energy released in the carbonator corresponds to the maximum possible heat retrieval. When EP is low and there is solar resource available (6–8 h and 14–17 h), the energy is stored, although due to the heat exchanger of the systems part of the energy could be used and $\dot{Q}_{AV}$ is bigger than $\dot{Q}_{CR}$. This storage stage remains in operation during the whole period as the solar resource extend up to 19 h. The available energy daily incomes achieved by $SP_{EP,min}$ (21,411.35 €/day) are almost 70 % higher than $AU_{EP,min}$ (see Fig. A.1 and Table A.1 in Appendix, 12,711.13 €/day).

The thermal energy production (Fig. 7a) and the incomes (Fig. 7b) for the representative day with the maximum daily average EP autumn ($AU_{EP,max}$) are illustrated in Fig. 7. In this case the EP is nearly constant during the majority of the day leading to a different operating scheme. Again, it is evident that the operation follows the EP pattern. During the first hours of operation, stored energy must be retrieved to operate the carbonator until solar resource is available to generate further CaO and CO_2. The carbonator is off between 14 and 16 h to save stored energy to be retrieved when the electricity price is increased by the end of the day. As available solar resource is strongly reduced and EP decays at 17 h, the whole system is switch off. Then, the system is switch on to operate between 18 and 20 h at elevated EP. The highest available energy daily incomes are again achieved for the $SP_{EP,max}$ (see Fig. A.2 and Table A.1),

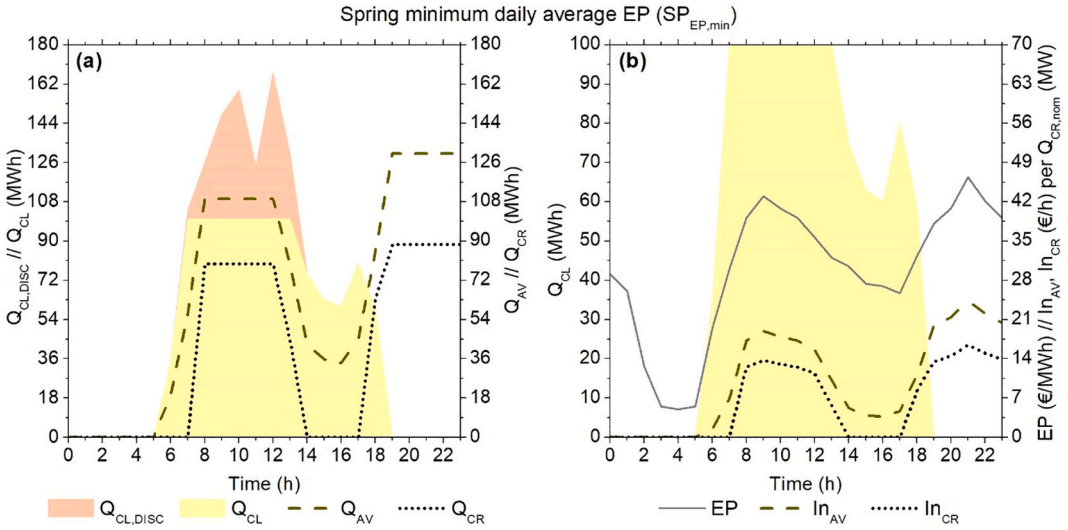

Fig. 6. Energy production (a) and incomes (b) under spring minimum daily average EP ($SP_{EP,min}$).

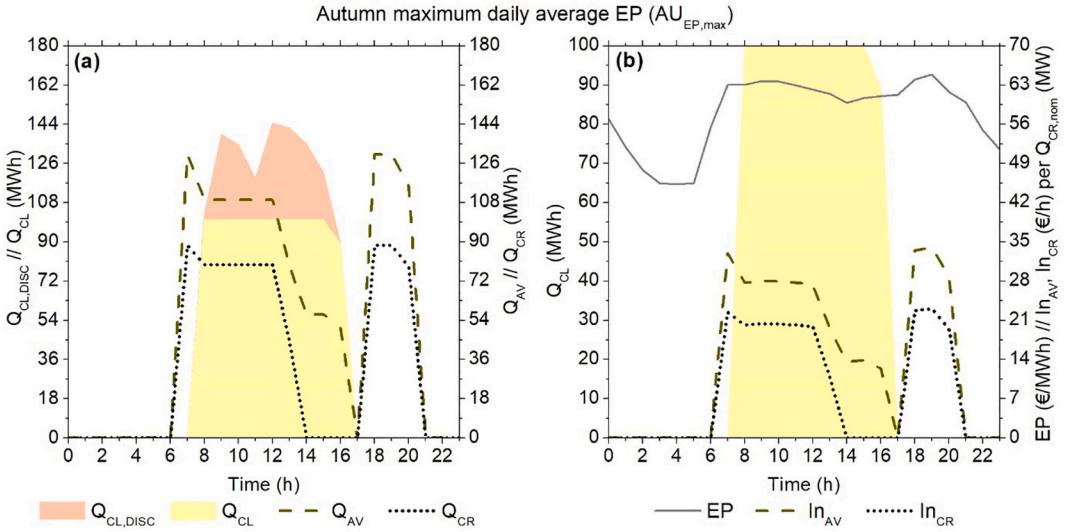

Fig. 7. Energy production (a) and incomes (b) under autumn maximum daily average EP ($AU_{EP,max}$).

18 % greater than $AU_{EP,max}$ (28,943.56 €/day).

Figs. 8 and 9 illustrate the hourly thermal energy production for winter and summer under minimum and maximum DNI (complemented with the information in Appendix: summer minimum DNI ($SU_{DNI,min}$) in Fig. A.3 and winter maximum DNI ($WI_{DNI,max}$) in Fig. A.4). During the representative day with the minimum daily average DNI for winter ($WI_{DNI,min}$), the system stores energy during the whole period with available solar resource to retrieve the energy at around 18 h when the maximum EP of the day is found. In this case, the solar radiation pattern is remarkably irregular with sharp variations between consecutive hours. It is observed that, the less daily solar radiation, the greater the concentration of energy production in certain hours. As previously highlighted, the storage stage also releases available thermal energy ($\dot{Q}_{AV} > 0$). These profiles allow to size the storage system as presented latter in the manuscript. The comparison between representative days with minimum DNI in summer (Appendix Fig. A.3 and Table A.1) and winter show an expected and abrupt difference of daily incomes; being 186 % greater in summer (16,692.81 €/day) than in winter (5826.95 €/day).

Finally, Fig. 9 show the most favourable case: summer representative day with maximum daily average DNI under a smooth hourly EP scenario. Energy production is shown in Fig. 9a while incomes are illustrated in Fig. 9b. There is a delay in the performance of the system to adjust to the maximum EP. The storage of energy begins at 6 h while the carbonator is started up at 8 h and shutted down by the end of the day (23 h). The highest available energy total incomes are achieved by $SU_{DNI,max}$ (33,363.56 €/day), being 17 % greater than $WI_{DNI,max}$ day (see Fig. A.4 and Table A.1 in Appendix).

As observed under every representative day, the methodology implemented to maximize the daily incomes promotes a distribution of energy production in those hours with the highest electricity prices. The energy retrieval is concentrated in those hours with the highest EP. With high solar resource availability and a uniform EP profile, the energy production is the greatest with minimum operational outages in the carbonator. However, with sharp variations of EP, the energy production is concentrated in the highest EP peak or peaks, which tend to be concentrated early in the morning (8 h) or/and at the end of the day (21 h). Regarding the available energy ($\dot{Q}_{AV}$), the CaL TCES system only releases energy from heat exchangers EE-CaO, EE-CaO-P and EE-CO2 (see Fig. 1) under full storage mode with the carbonator off. Thus, if the carbonator operates from sunset to the end of the day due to high hourly EP, the CaL TCES system can release energy continuously from

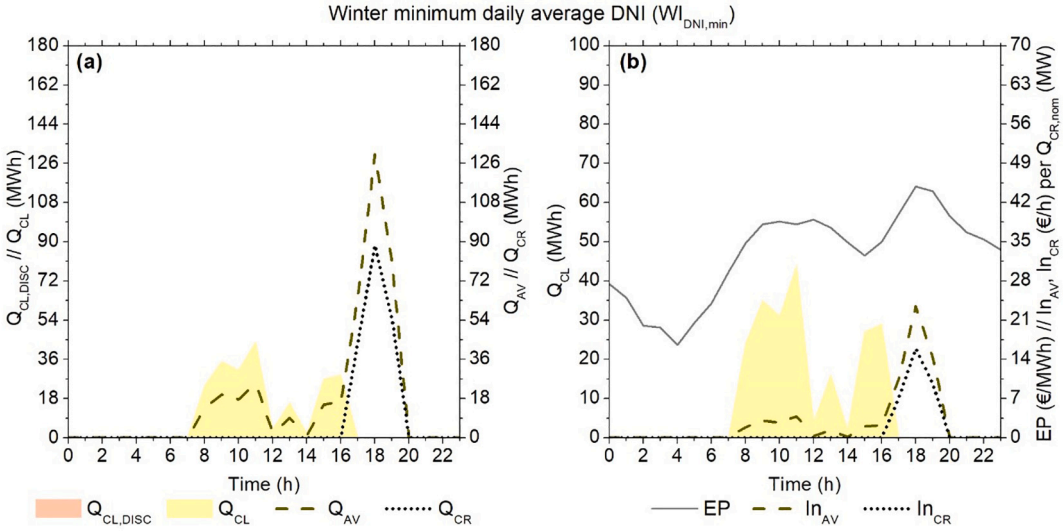

Fig. 8. Energy production (a) and incomes (b) under winter minimum daily average DNI ($WI_{DNI,min}$).

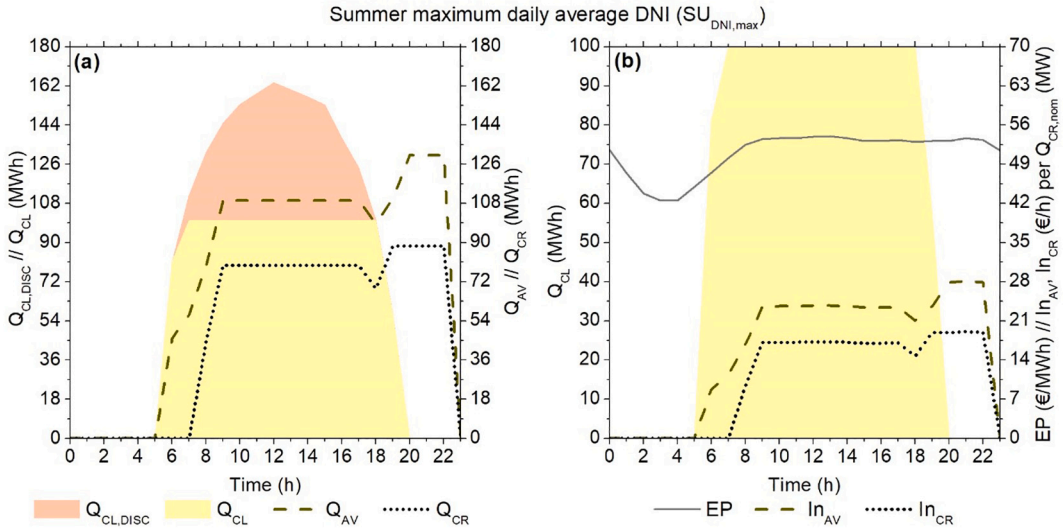

Fig. 9. Energy production (a) and incomes (b) under summer maximum daily average DNI ($SU_{DNI,max}$).

sunrise to the end of the day.

4.2. Daily storage profiles of gas and solids

With the obtained results, it is possible to determine the hourly amount of CO_2, lime and limestone stored under each representative day. Two representative cases corresponding to Winter minimum daily average DNI and Autumn maximum daily average EP are shown in Figs. 10 and 11 while the whole set of figures for the rest of representative days is included in the Appendix (see Figs. A.5, A.6, A.7, A.8, A.13 and A.14).

The left plots represent the daily profiles of calciner/carbonator loads and storage/discharge loads. The calciner load (L_{CL}) is represented by the yellow area. The discharge load (L_{dch}) covers the brown area. The sum of the calciner and the discharge load areas represents the total energy input supplied to the CaL TCES system. The storage load (L_{st}) corresponds to the striped area which represents the energy stored; the difference between the instantaneous solar energy and the energy released in the carbonator. The solid curve shows the daily carbonator load evolution. The total area covered by stored energy and carbonator heat release is equal to the energy supplied load (calciner heat and energy retrieved from storage tanks) to the system, considering energy losses. In the right plots, the calciner and carbonator loads are represented by the yellow area and the black solid line, respectively. The dashed-dotted curve illustrates the daily variation of the CO_2 volume in the Storage Tank ST3 and the dashed curve presents the daily profile of CaO volume in the Storage Tank ST2. The evolution of the volume stored of limestone in the Storage Tank ST1 is represented by the dotted curve.

Fig. 10b shows the hourly amount of CO_2, lime and limestone stored and their variation along the day for $AU_{EP,max}$. Initially, tanks are partially loaded and this stored energy is retrieved during the first operational hours (6 h–7 h) as illustrated in Fig. 7. The Storage Tanks ST2 and ST3 (V_{CaO}, V_{CO2}) are completely emptied during this period. Once solar resource is available, those tanks are progressively re-filled while ST1 (V_{CaCO3}) is emptied. At 16 h a maximum stored volume is reached for ST2 and ST3 (V_{CaO}, V_{CO2}) and this energy is retrieved in the following hours. These maximum stored volumes are significant values for the design and sizing of the CaO and CO_2 tanks. The same happens with the $CaCO_3$ tank at 7 h where the maximum required volume is achieved. Table 2 shows the maximum volume achieve during each day selected for the operating methodology assessment.

The daily storage/discharge energy loads (Fig. 11a) and the

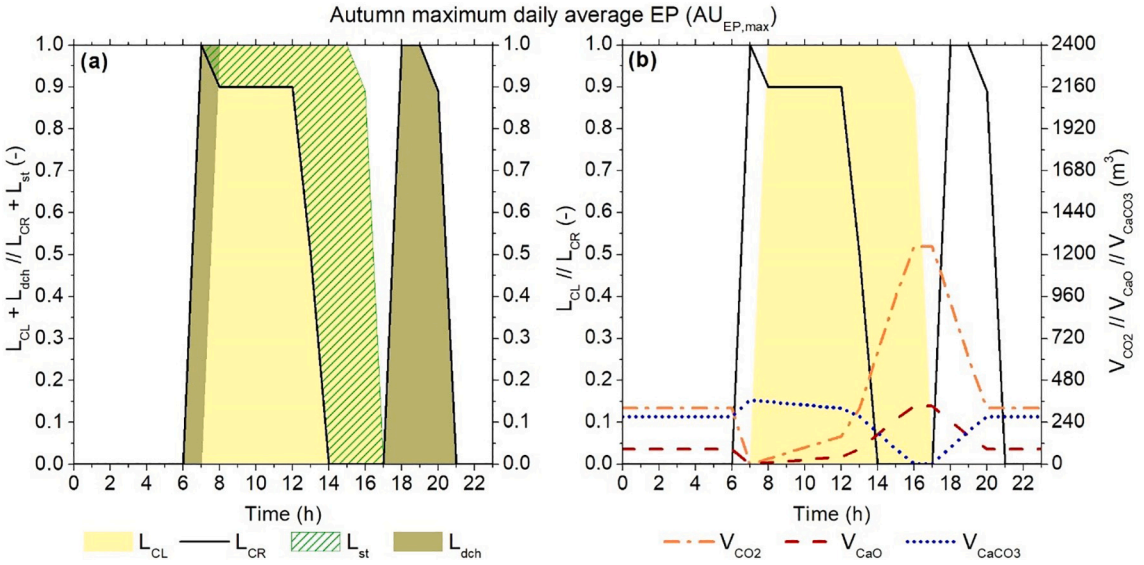

Fig. 10. Energy storage/discharge profile (a) and volume profile of storage tanks (b) under autumn maximum daily average EP ($AU_{EP,max}$).

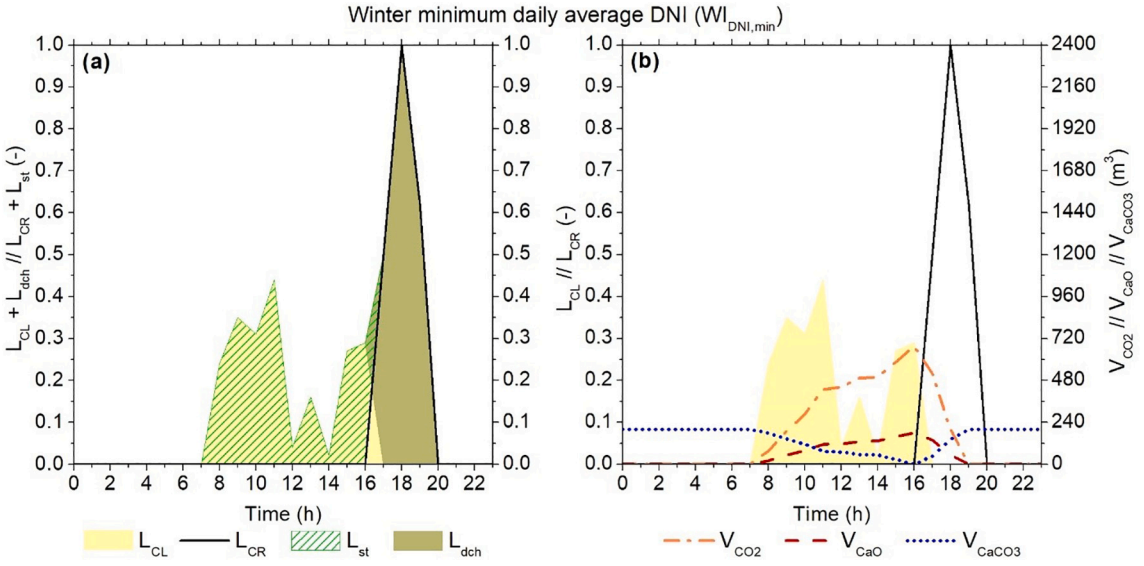

Fig. 11. Energy storage/discharge profile (a) and volume profile of storage tanks (b) under winter minimum daily average DNI ($WI_{DNI,min}$).

evolution of the storage level (Fig. 11b) for the representative day in winter with minimum daily average DNI ($WI_{DNI,min}$) are illustrated in Fig. 11. The energy is stored during the first sunlight hours (6–16 h) to be progressively retrieved along the rest of the day (16–19 h). The energy storage profile of the $WI_{DNI,min}$ day has lower maximum volumes stored than $AU_{EP,max}$ given the lower solar energy availability. Under $WI_{DNI,min}$, the largest stored volume of CO_2 and CaO are achieved at sunset (16 h).

The maximum stored volumes are reached in the $AU_{EP,min}$ representative day (see Fig. A.5 in Appendix), in which the energy is stored during practically all the hours with solar radiation availability. The limestone Storage Tank ST1 will require of at least 651.34 m^3 (1335.90 tons), analyzing the representative days selected. The maximum stored volume of limestone is 13 % lower than the maximum stored volume of a mixture of solids (1535 tons of CaO + $CaCO_3$) found in literature under the same calciner size (100 MWth) and operating conditions (950 °C and 1 bar) [53]. Besides, the maximum amount of CaO diverted to storage in a representative day with high daily DNI (1373 tons) appeared in Ortiz et al. [53] is 45.5 % lower than the maximum stored volume of lime under $AU_{EP,min}$ day (748.49 tons) assessed in the present work. Thus, the recirculation of unconverted CaO particles, proposed in Fig. 1, will minimize the size of the solids storage tanks (ST1 and ST2).

4.3. Daily operating pattern/sequence

Once the economically optimal operation points are found for the different hourly conditions of the facility, their representation upon the operation maps will allow to visualize the path and the evolution of the storage and discharge efficiencies along the day. The hourly operating points are represented as black dots upon the operation maps under ESOM (green area) and EROM (brown area) described elsewhere [55]. The calciner and carbonator loads are again represented by the yellow area and the black solid line, respectively.

The daily operation pattern under the representative days of spring minimum and autumn with maximum daily average EP ($SP_{EP,min}$ and $AU_{EP,max}$) are illustrated in Fig. 12. The operating profile during $SP_{EP,min}$ representative day changes. During the first hours of the day (0–7 h) the carbonator is disconnected. Thus, solar resource supplied in this period

Table 2
Maximum stored volumes per each representative day.

Summary of daily storage profiles results				
Representative days		Maximum stored volume		
		$CaCO_3$ (ST1)	CaO (ST2)	CO_2 (ST3)
		(m^3 // tons)		
Spring	$SP_{EP,min}$	485.87 // 996.52	438.93 // 550.90	1642.95 // 449.70
	$SP_{EP,max}$	378.85 // 777.02	427.81 // 536.94	1601.31 // 438.30
Autumn	$AU_{EP,min}$	651.34 // 1335.90	596.36 // 748.49	2232.23 // 610.99
	$AU_{EP,max}$	367.17 // 753.07	332.83 // 417.73	1245.82 // 340.99
Summer	$SU_{DNI,min}$	388.32 // 796.44	350.8 // 440.29	1313.08 // 359.41
	$SU_{DNI,max}$	324.86 // 666.29	293.48 // 368.35	1098.5 // 300.67
Winter	$WI_{DNI,min}$	198.11 // 406.32	181.39 // 227.66	678.96 // 185.84
	$WI_{DNI,max}$	426.21 // 874.16	385.03 // 483.25	1441.18 // 394.47

is fully stored (CL load is 35 % at 6 h and CL operates at 100 % at 7 h). From 8 to 12 h, CL operates at full load and CR at 90 % storing energy with high efficiency, the highest energy storage efficiency (see Fig. A.15a in Appendix, 74 %) is achieved at 13 h. The carbonator is again shutted down during the next 4 h (14–17 h) and, is again operative to retrieved thermal energy during the rest of the day (18–23 h). The maximum energy availability efficiency (see Fig. A.15a in Appendix, 93 %) under $SP_{EP,min}$ day is reached during sunlight hours when the calciner/carbonator load difference is minimum (8–13 h). Regarding the operating hours under $AU_{EP,max}$, the carbonator is disconnected during the first part of the day (0–6 h) but at 7 h the CaL TCES system operates within the full energy retrieval mode. The operation continues under ESOM from 8 to 13 h, reaching the highest energy storage efficiency (Appendix Fig. A.15b, 74 %) at 13 h as in $SP_{EP,min}$. The carbonator is off for the next 3 h operating the system at full storage operation mode (14–16 h), while retrieving energy again from 18 to 20 h. The last part of the day the whole CaL TCES system is shutted down (21−23 h). The maximum availability energy efficiency (Appendix Fig. A.15b, 93 %) is reached during sunlight hours when the calciner/carbonator load difference is minimum.

The system performance for the representative days in summer with maximum DNI and in winter with minimum DNI is showed in Fig. 13. Under the $SU_{DNI,max}$ representative day, the carbonator operates from 7 h to the end of the day, being shutted down during the beginning of the day. The CaL TCES system stores energy from 5 to 7 h as in $SP_{EP,min}$ at full storage mode and between 7 and 18 h at ESOM, reaching the highest energy storage efficiency (Appendix Fig. A.16a, 75 %) at 18 h. The last part of the day the system retrieves energy to be eventually disconnected at 23 h. The operating profile under $WI_{DNI,min}$ goes to the extreme situations, the TCES system store energy or release energy under full modes (only storage or retrieval of energy, not combined operation). It only operates under EROM between 16 and 18 h while the rest of the day it operates within the full storage mode or the system is completely disconnected. The highest energy storage efficiency (see Fig. A.16b in Appendix, 64 %) is achieved during all the sunlight period for $WI_{DNI,min}$. The maximum availability energy efficiency (see Fig. A.16b in Appendix, 68 %) is reached when carbonator operates.

Summarizing operational behavior, the more solar energy availability, the greater number of operation hours under energy storage mode. If the high EP during a representative day is concentrated in the second part of the day, the full energy storage accumulates from the beginning of the day to the first hour of carbonator starts its operation. Under energy retrieval mode, the maximum energy availability efficiency is reached when the difference between carbonator/calciner loads is minimum (see Figs. A.15 and A.16 in Appendix).

5. Conclusions

The novelty of this study relies in the definition of a methodology to determine the daily dynamic operation of a CaL TCES system to maximize the incomes received from the sale of electricity. The economic optimization methodology has been applied to eight representative days within a year using a Genetic method. The selected days cover minimum and maximum daily average EP for spring and autumn seasons and DNI during summer and winter periods, meeting the criteria defined for the selection of these representative days. The daily incomes is the target variable of the optimization problem. Other results obtained from the optimization are the daily energy production and the volume needed in the gas and solids storage tanks.

Regarding the thermal energy production, the highest hourly incomes will be obtained during the hours with maximum EP. The higher number of maximum EP peaks during a day, the higher the

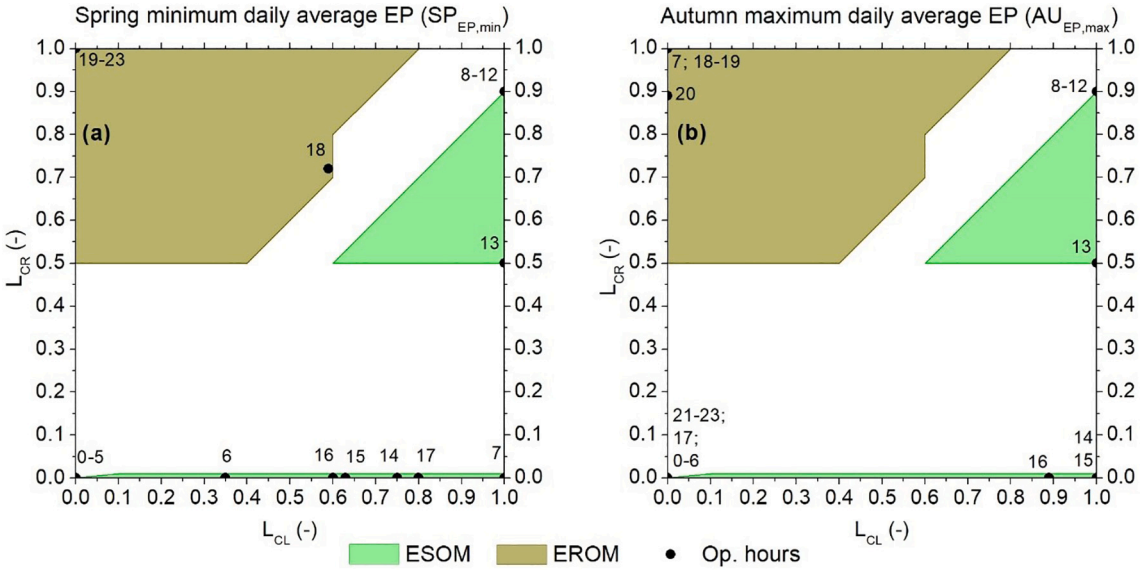

Fig. 12. Comparison of the operation sequence under spring minimum ((a) $SP_{EP,min}$) and autumn maximum ((b) $AU_{EP,max}$) daily average EP.

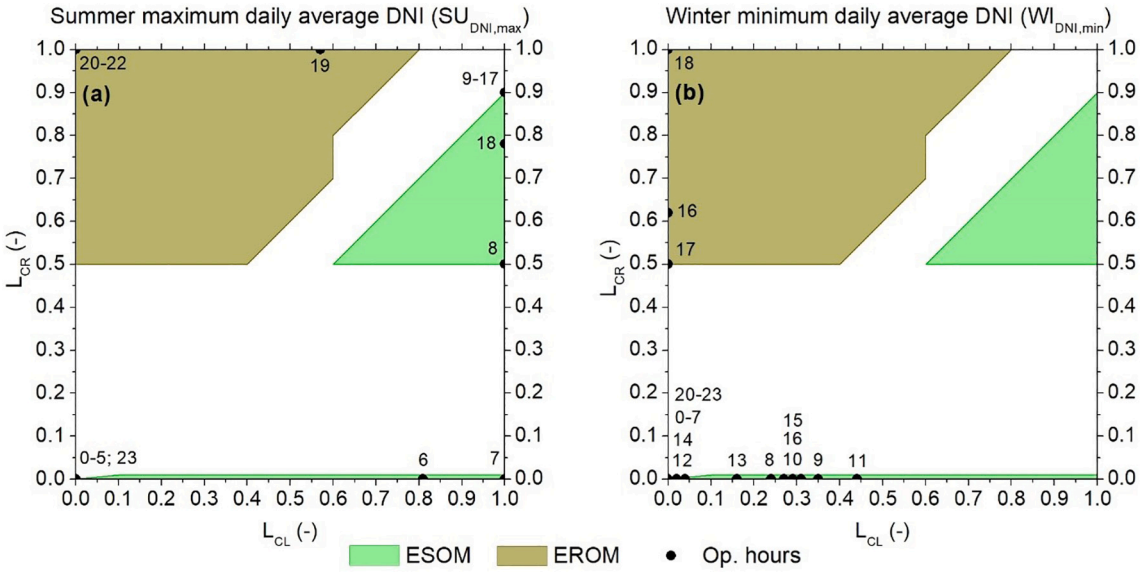

Fig. 13. Comparison of the operation sequence under summer maximum ((a) $SU_{DNI,max}$) and winter minimum ((b) $WI_{DNI,min}$) daily average DNI.

concentration of the energy production within short periods of time. The thermal energy is retrieved uniformly from the CaL TCES system for longer periods when the daily EP gap is very narrow. Besides, the days with minimum daily average DNI have a solar energy availability profile with sharp variations between consecutive hours. Thus, the energy production within those days will have a greater slack between hours. However, the higher the daily average DNI, the greater the stability of the energy production for a longer period.

The assessment of the daily evolution of the gas and solids volume stored will determine the minimum volume required in the design and construction of each Storage Tank. The minimum required size of the storage tanks will be found during a representative day in which (i) the carbonator only release energy within the period between sunset and the end of the day and (ii) the energy is stored during all the sunlight hours. Within any representative day, the maximum stored volume of lime and CO_2 will be found at sunset, whereas the maximum stored volume of limestone will be achieved at the beginning and the end of the day. Besides, if the carbonator load is below the calciner load, the surplus of solar energy at calciner receiver will be stored. The energy is mostly retrieved from the storage tanks of CaO and CO_2 within the last part of the day without solar radiation to cover the carbonator energy demand. The implementation of the SSU in the CaL TCES system will minimize the Storage Tank size related to lime and limestone, comparing with data found in literature.

Nomenclature

Symbols

E	thermal energy, MWh or GWh
f	fraction, –
h	hour, h
In	Incomes, €
k	CaO deactivation constant, –
L	load, –
$\dot{m}$	mass flow rate, kg/s
$\dot{Q}$	heat flow rate, MW
r	fraction of CaO particles, –
R	molar ratio CaO/CO_2, –
V	volume, m^3
X	conversion, –
ΔH_R^0	enthalpy of carbonation, kJ/mol
ε	void fraction, –
η	efficiency, –
ρ	density, kg/m^3

Subscripts and superscripts

av	thermal energy availability
AV	available
ave	average
BoD	Beginning of the Day
capt	carbon capture
CR	carbonator
CL	calciner
d	daily
dch	discharge or discharged
disc	discarded
EoD	End of the Day
g	gas
h	hourly
max	maximum
min	minimum
N	number carbonation-calcination cycles
nom	nominal
opt	optical
p	purge or particle
part	partial load
r	residual
s	solid
SOLAR	solar availability at calciner receiver
SRPC	Steam Rankine Power Cycle
st	storage or stored
ther	thermal
y	yearly

Acronyms and abbreviations

AU	Autumn
CaL	Calcium-looping
CSP	Concentrating Solar Power
DNI	Direct Normal Irradiation
EE	Energy Emitted
EP	Electricity Price

ER	Energy Required
EROM	Energy Retrieval Operation Mode
ESOM	Energy Storage Operation Mode
EES	Engineering Equation Solver
FB	Fluidized Bed
HE	Heat Exchanger
IEA	International Energy Agency
IGN	Instituto Geográfico Nacional
NCAR	National Center for Atmospheric Research
PV	Photovoltaic
PVGIS	Photovoltaic Geographical Information System
REE	Red Eléctrica Española
SFA	Solar Field Area
SP	Spring
SSU	Solids Separation Unit
ST	Storage Tank
SU	Summer
TCES	Thermochemical Energy Storage
TMY	Typical Meteorological Year
WI	Winter

CRediT authorship contribution statement

Sara Pascual: Simulation activities; Methodology; Writing; Revision
Luis M. Romeo: Conceptualization; Methodology; Revision; Funding acquisition
Pilar Lisbona: Conceptualization; Methodology; Writing; Revision

Declaration of competing interest

The authors declare that they have no known competing financial interests or personal relationships that could have appeared to influence the work reported in this paper.

Data availability

Data will be made available on request.

Acknowledgments

The FPU Programme of the Spanish Ministry of Science, Innovation and Universities (FPU 2017/03902) provided financial support for S.P. Ph.D. studies. The research was funded by the EU Horizon 2020 research and innovation programme [GA No 727348], SOCRATCES project. The work described in this paper is supported by the Government of Aragon and cofinanced by FEDER 2014–2020 “Construyendo Europa desde Aragón” (Research Group DGA T46_20R).

Appendix A. Supplementary data

Supplementary data to this article can be found online at https://doi.org/10.1016/j.est.2023.107587.

References

[1] S. Michalski, D.P. Hanak, V. Manovic, Advanced power cycles for coal-fired power plants based on calcium looping combustion: a techno-economic feasibility assessment, Appl. Energy 269 (2020), 114954, https://doi.org/10.1016/j.apenergy.2020.114954.
[2] L.M. Romeo, D. Catalina, P. Lisbona, Y. Lara, A. Martínez, Reduction of greenhouse gas emissions by integration of cement plants, power plants, and CO2 capture systems, Greenhouse GasesSci. Technol. (2011) 1, https://doi.org/10.1002/ghg3.5.
[3] M. Haaf, R. Anantharaman, S. Roussanaly, J. Ströhle, B. Epple, CO2 capture from waste-to-energy plants: techno-economic assessment of novel integration concepts of calcium looping technology, Resour. Conserv. Recycl. 162 (2020), 104973, https://doi.org/10.1016/j.resconrec.2020.104973.
[4] M.E. Diego, M. Alonso, Operational feasibility of biomass combustion with in situ CO2 capture by CaO during 360 h in a 300 kWth calcium looping facility, Fuel 181 (2016) 325–329, https://doi.org/10.1016/j.fuel.2016.04.128.
[5] R. Barker, The reactivity of calcium oxide towards carbon dioxide and its use for energy storage, Appl. Chem. Biotechnol. 24 (1974) 221–227.
[6] International Energy Agency, Net Zero by 2050: A Roadmap for the Global Energy Sector, 2021.
[7] X. Chen, Z. Zhang, C. Qi, X. Ling, H. Peng, State of the art on the high-temperature thermochemical energy storage systems, Energy Convers. Manag. 177 (2018) 792–815, https://doi.org/10.1016/j.enconman.2018.10.011.
[8] A.A. Khosa, T. Xu, B.Q. Xia, J. Yan, C.Y. Zhao, Technological challenges and industrial applications of CaCO3/CaO based thermal energy storage system – a review, Sol. Energy 193 (2019) 618–636, https://doi.org/10.1016/j.solener.2019.10.003.
[9] G.S. Grasa, J.C. Abanades, CO2 capture capacity of CaO in long series of carbonation/calcination cycles, Ind. Eng. Chem. Res. 45 (2006) 8846–8851, https://doi.org/10.1021/ie0606946.
[10] A. Perejón, L.M. Romeo, Y. Lara, P. Lisbona, A. Martínez, J.M. Valverde, The calcium-looping technology for CO2 capture: on the important roles of energy integration and sorbent behavior, Appl. Energy (2016) 162, https://doi.org/10.1016/j.apenergy.2015.10.121.
[11] P. Lisbona, M. Bailera, T. Hills, M. Sceats, L.I. Díez, L.M. Romeo, Energy consumption minimization for a solar lime calciner operating in a concentrated solar power plant for thermal energy storage, Renew. Energy 156 (2020) 1019–1027, https://doi.org/10.1016/j.renene.2020.04.129.
[12] C. Ortiz, J.M. Valverde, R. Chacartegui, L.A. Perez-Maqueda, Carbonation of limestone derived CaO for thermochemical energy storage: from kinetics to process integration in concentrating solar plants, ACS Sustain. Chem. Eng. 6 (2018) 6404–6417, https://doi.org/10.1021/acssuschemeng.8b00199.
[13] I. Sarbu, C. Sebarchievici, A comprehensive review of thermal energy storage, MDPI Sustain. 10 (2018) 1–32, https://doi.org/10.3390/su10010191.
[14] D. Liu, L. Xin-Feng, L. Bo, Z. Si-quan, X. Yan, Progress in thermochemical energy storage for concentrated solar power: a review, Int. J. Energy Res. 42 (2018) 4546–4561, https://doi.org/10.1002/er.4183.
[15] G. Alva, Y. Lin, G. Fang, An overview of thermal energy storage systems, Energy 144 (2018) 341–378, https://doi.org/10.1016/j.energy.2017.12.037.
[16] M. Benitez-guerrero, B. Sarrion, A. Perejon, P.E. Sanchez-jimenez, L.A. Perez-maqueda, J. Manuel, Large-scale high-temperature solar energy storage using natural minerals, Sol. Energy Mater. Sol. Cells 168 (2017) 14–21, https://doi.org/10.1016/j.solmat.2017.04.013.
[17] M. Benitez-guerrero, J. Manuel, P.E. Sanchez-jimenez, A. Perejon, L.A. Perez-maqueda, Multicycle activity of natural CaCO 3 minerals for thermochemical energy storage in concentrated solar power plants, Sol. Energy 153 (2017) 188–199, https://doi.org/10.1016/j.solener.2017.05.068.
[18] C. Tregambi, F. Di Lauro, F. Montagnaro, P. Salatino, R. Solimene, 110th anniversary: calcium looping coupled with concentrated solar power for carbon capture and thermochemical energy storage, Ind. Eng. Chem. Res. 58 (2019) 21262–21272, https://doi.org/10.1021/acs.iecr.9b03083.
[19] J.M. Valverde, P.E. Sanchez-Jimenez, A. Perejon, L.A. Perez-Maqueda, Role of looping-calcination conditions on self-reactivation of thermally pretreated CO2 sorbents based on CaO, Energy Fuels 27 (2013) 3373–3384, https://doi.org/10.1021/ef400480j.
[20] J.M. Valverde, A model on the CaO multicyclic conversion in the Ca-looping process, Chem. Eng. J. 228 (2013) 1195–1206, https://doi.org/10.1016/j.cej.2013.05.023.
[21] M. Sayyah, Y. Lu, R.I. Masel, K.S. Suslick, Mechanical activation of CaO-based adsorbents for CO2 capture, ChemSusChem 6 (2013) 193–198, https://doi.org/10.1002/cssc.201200454.
[22] M. Benitez-Guerrero, J.M. Valverde, A. Perejon, P.E. Sanchez-Jimenez, L.A. Perez-Maqueda, Effect of milling mechanism on the CO2 capture performance of limestone in the calcium looping process, Chem. Eng. J. 346 (2018) 549–556, https://doi.org/10.1016/j.cej.2018.03.146.
[23] F. Di Lauro, C. Tregambi, F. Montagnaro, P. Salatino, R. Chirone, R. Solimene, Improving the performance of calcium looping for solar thermochemical energy storage and CO2 capture, Fuel (2021) 298, https://doi.org/10.1016/j.fuel.2021.120791.
[24] A. Coppola, A. Esposito, F. Montagnaro, G. De Tommaso, F. Scala, P. Salatino, Effect of exposure to SO2 and H2O during the carbonation stage of fluidised bed calcium looping on the performance of sorbents of different nature, Chem. Eng. J. 377 (2019), 120626, https://doi.org/10.1016/j.cej.2018.12.086.
[25] C. Tregambi, P. Salatino, R. Solimene, F. Montagnaro, An experimental characterization of calcium looping integrated with concentrated solar power, Chem. Eng. J. (2017), https://doi.org/10.1016/j.cej.2017.08.068.
[26] H. Guo, S. Wang, C. Li, Y. Zhao, Q. Sun, X. Ma, Incorporation of Zr into calcium oxide for CO2 capture by a simple and facile sol-gel method, Ind. Eng. Chem. Res. 55 (2016) 7873–7879, https://doi.org/10.1021/acs.iecr.5b04112.
[27] A. Antzara, E. Heracleous, A.A. Lemonidou, Improving the stability of synthetic CaO-based CO2 sorbents by structural promoters, Appl. Energy 156 (2015) 331–343, https://doi.org/10.1016/j.apenergy.2015.07.026.
[28] M. Benitez-Guerrero, J.M. Valverde, P.E. Sanchez-Jimenez, A. Perejon, L.A. Perez-Maqueda, Calcium-looping performance of mechanically modified Al2O3-CaO composites for energy storage and CO2 capture, Chem. Eng. J. 334 (2018) 2343–2355, https://doi.org/10.1016/j.cej.2017.11.183.
[29] J.M. Valverde, M. Barea-López, A. Perejón, P.E. Sánchez-Jiménez, L.A. Pérez-Maqueda, Effect of thermal pretreatment and nanosilica addition on limestone performance at calcium-looping conditions for thermochemical energy storage of

concentrated solar power, Energy Fuels 31 (2017) 4226–4236, https://doi.org/10.1021/acs.energyfuels.6b03364.
[30] J. Arcenegui-Troya, P.E. Sánchez-Jiménez, A. Perejón, V. Moreno, J.M. Valverde, L.A. Pérez-Maqueda, Kinetics and cyclability of limestone (CaCO3) in presence of steam during calcination in the CaL scheme for thermochemical energy storage, Chem. Eng. J. (2021) 417, https://doi.org/10.1016/j.cej.2021.129194.
[31] J. Arcenegui-Troya, P.E. Sánchez-Jiménez, A. Perejón, J.M. Valverde, L.A. Pérez-Maqueda, Steam-enhanced calcium-looping performance of limestone for thermochemical energy storage: the role of particle size, J. Energy Storage (2022) 51, https://doi.org/10.1016/j.est.2022.104305.
[32] Y. Da, Y. Xuan, L. Teng, K. Zhang, X. Liu, Y. Ding, Calcium-based composites for direct solar-thermal conversion and thermochemical energy storage, Chem. Eng. J. (2020), https://doi.org/10.1016/j.cej.2019.122815.
[33] L. André, S. Abanades, Evaluation and performances comparison of calcium, strontium and barium carbonates during calcination/carbonation reactions for solar thermochemical energy storage, J. Energy Storage 13 (2017) 193–205, https://doi.org/10.1016/j.est.2017.07.014.
[34] D. Choi, A.-H. Alissa Park, Y. Park, Effects of eutectic alkali chloride salts on the carbonation reaction of CaO-based composites for potential application to a thermochemical energy storage system, Chem. Eng. J. 437 (2022), 135481, https://doi.org/10.1016/j.cej.2022.135481.
[35] K.T. Møller, T.D. Humphries, A. Berger, M. Paskevicius, C.E. Buckley, Thermochemical energy storage system development utilising limestone, Chem. Eng. J. Adv. 8 (2021), 100168, https://doi.org/10.1016/j.ceja.2021.100168.
[36] Y. Yang, Y. Li, X. Yan, J. Zhao, C. Zhang, Development of thermochemical heat storage based on CaO/CaCO3 cycles: a review, Energies (2021) 14, https://doi.org/10.3390/en14206847.
[37] B. Sarrión, A. Perejón, P.E. Sánchez-Jiménez, L.A. Pérez-Maqueda, J.M. Valverde, Role of calcium looping conditions on the performance of natural and synthetic ca-based materials for energy storage, J. CO2Util. (2018), https://doi.org/10.1016/j.jcou.2018.10.018.
[38] L. Yang, G. Huang, Z. Huang, Optimized design of Ca-based thermochemical heat storage materials for concentrated solar power, J. Energy Storage 43 (2021), 103236, https://doi.org/10.1016/j.est.2021.103236.
[39] H. Zheng, X. Liu, Y. Xuan, C. Song, D. Liu, Q. Zhu, et al., Thermochemical heat storage performances of fluidized black CaCO3 pellets under direct concentrated solar irradiation, Renew. Energy 178 (2021) 1353–1369, https://doi.org/10.1016/j.renene.2021.07.026.
[40] C. Ortiz, A. Carro, R. Chacartegui, J.M. Valverde, Low-pressure calcination to enhance the calcium looping process for thermochemical energy storage, J. Clean. Prod. (2022) 363, https://doi.org/10.1016/j.jclepro.2022.132295.
[41] O. Achkari, A. El Fadar, Latest developments on TES and CSP technologies – energy and environmental issues, applications and research trends, Appl. Therm. Eng. 167 (2020), 114806, https://doi.org/10.1016/j.applthermaleng.2019.114806.
[42] C. Prieto, P. Cooper, A.I. Fernández, L.F. Cabeza, Review of technology: thermochemical energy storage for concentrated solar power plants, Renew. Sust. Energ. Rev. 60 (2016) 909–929, https://doi.org/10.1016/j.rser.2015.12.364.
[43] P. Pan, M. Zhang, G. Xu, H. Chen, X. Song, T. Liu, Thermodynamic and economic analyses of a new waste-to-energy system incorporated with a biomass-fired power plant, Energies (2020) 13, https://doi.org/10.3390/en13174345.
[44] G. Colelli, R. Chacartegui, C. Ortiz, A. Carro, A.P. Arena, V. Verda, Life cycle and environmental assessment of calcium looping (CaL) in solar thermochemical energy storage, Energy Convers. Manag. 257 (2022), 115428, https://doi.org/10.1016/j.enconman.2022.115428.
[45] I. Arias, J. Cardemil, E. Zarza, L. Valenzuela, R. Escobar, Latest developments, assessments and research trends for next generation of concentrated solar power plants using liquid heat transfer fluids, Renew. Sust. Energ. Rev. 168 (2022), 112844.
[46] U. Tesio, E. Guelpa, V. Verda, Comparison of sCO2 and He Brayton cycles integration in a calcium-looping for concentrated solar power, Energy 247 (2022), 123467, https://doi.org/10.1016/j.energy.2022.123467.
[47] C. Ortiz, R. Chacartegui, J.M. Valverde, A. Alovisio, J.A. Becerra, Power cycles integration in concentrated solar power plants with energy storage based on calcium looping, Energy Convers. Manag. 149 (2017) 815–829, https://doi.org/10.1016/j.enconman.2017.03.029.
[48] S. Pascual, P. Lisbona, M. Bailera, L.M. Romeo, Design and operational performance maps of calcium looping thermochemical energy storage for concentrating solar power plants, Energy 220 (2021), 119715, https://doi.org/10.1016/j.energy.2020.119715.
[49] R. Bravo, C. Ortiz, R. Chacartegui, D. Friedrich, Hybrid solar power plant with thermochemical energy storage: a multi-objective operational optimisation, Energy Convers. Manag. 205 (2020), 112421, https://doi.org/10.1016/j.enconman.2019.112421.
[50] R. Bravo, C. Ortiz, R. Chacartegui, D. Friedrich, Multi-objective optimisation and guidelines for the design of dispatchable hybrid solar power plants with thermochemical energy storage, Appl. Energy (2021) 282, https://doi.org/10.1016/j.apenergy.2020.116257.
[51] C. Tregambi, P. Bareschino, E. Mancusi, F. Pepe, F. Montagnaro, R. Solimene, et al., Modelling of a concentrated solar power – photovoltaics hybrid plant for carbon dioxide capture and utilization via calcium looping and methanation, Energy Convers. Manag. 230 (2021), 113792, https://doi.org/10.1016/j.enconman.2020.113792.
[52] C. Ortiz, R. Chacartegui, J.M. Valverde, A. Carro, C. Tejada, J. Valverde, Increasing the solar share in combined cycles through thermochemical energy storage, Energy Convers. Manag. 229 (2021), 113730, https://doi.org/10.1016/j.enconman.2020.113730.
[53] C. Ortiz, C. Tejada, R. Chacartegui, R. Bravo, A. Carro, J.M. Valverde, et al., Solar combined cycle with high-temperature thermochemical energy storage, Energy Convers. Manag. 241 (2021), 114274, https://doi.org/10.1016/j.enconman.2021.114274.
[54] S. Pascual, Lauro F. Di, P. Lisbona, L.M. Romeo, C. Tregambi, F. Montagnaro, et al., Improvement of performance of fluidized bed calcium looping for thermochemical solar energy storage: modelling and experiments, in: Proc 10th Eur Combust Meet, 2021, pp. 1430–1435.
[55] S. Pascual, P. Lisbona, L.M. Romeo, Operation maps in calcium looping thermochemical energy storage for concentrating solar power plants, J. Energy Storage 55 (2022), 105771, https://doi.org/10.1016/j.est.2022.105771.
[56] G. Martinez Castilla, D.C. Guío-Pérez, S. Papadokonstantakis, D. Pallarès, F. Johnsson, Techno-economic assessment of calcium looping for thermochemical techno-economic assessment of calcium looping for thermochemical energy storage with CO2 capture, Energies 14 (2021) 0–17.
[57] C. Ortiz, J.M. Valverde, R. Chacartegui, L.A. Perez-Maqueda, P. Giménez, The calcium-looping (CaCO3/CaO) process for thermochemical energy storage in concentrating solar power plants, Renew. Sust. Energ. Rev. 113 (2019), 109252, https://doi.org/10.1016/j.rser.2019.109252.
[58] European Commission, PVGIS - photovoltaic geographical information system. https://ec.europa.eu/jrc/en/pvgis, 2021 (accessed October 4, 2021).
[59] F. Rinaldi, M. Binotti, A. Giostri, G. Manzolini, Comparison of linear and point focus collectors in solar power plants, Energy Procedia 49 (2013) 1491–1500, https://doi.org/10.1016/j.egypro.2014.03.158.
[60] V. Manovic, J.P. Charland, J. Blamey, P.S. Fennell, D.Y. Lu, E.J. Anthony, Influence of calcination conditions on carrying capacity of CaO-based sorbent in CO2 looping cycles, Fuel 88 (2009) 1893–1900, https://doi.org/10.1016/j.fuel.2009.04.012.
[61] R. Chacartegui, A. Alovisio, C. Ortiz, J.M. Valverde, V. Verda, J.A. Becerra, Thermochemical energy storage of concentrated solar power by integration of the calcium looping process and a CO2 power cycle, Appl. Energy 173 (2016) 589–605, https://doi.org/10.1016/j.apenergy.2016.04.053.
[62] L.M. Romeo, Y. Lara, P. Lisbona, J.M. Escosa, Optimizing make-up flow in a CO2 capture system using CaO, Chem. Eng. J. 147 (2009) 252–258, https://doi.org/10.1016/j.cej.2008.07.010.
[63] J.P. Rincon Duarte, D. Kriechbaumer, B. Lachmann, S. Tescari, T. Fend, M. Roeb, et al., Solar calcium looping cycle for CO2 capturing in a cement plant. Definition of process parameters and reactors selection, Sol. Energy 238 (2022) 189–202, https://doi.org/10.1016/j.solener.2022.04.031.
[64] N. Rodriguez, M. Alonso, J.C. Abanades, A. Charitos, C. Hawthorne, G. Scheffknecht, et al., Comparison of experimental results from three dual fluidized bed test facilities capturing CO2 with CaO, Energy Procedia 4 (2011) 393–401, https://doi.org/10.1016/j.egypro.2011.01.067.
[65] A. Charitos, N. Rodríguez, C. Hawthorne, M. Alonso, M. Zieba, B. Arias, et al., Experimental validation of the calcium looping CO2 capture process with two circulating fluidized bed carbonator reactors, Ind. Eng. Chem. Res. 50 (2011) 9685–9695, https://doi.org/10.1021/ie200579f.
[66] F-Chart, Genetic Method. Engineering Equation Solver (EES) Software. https://fchartsoftware.com/ees/, 2021 (accessed October 4, 2021).
[67] Red Eléctrica de España, PVPC | ESIOS electricidad · datos · transparencia. https://www.esios.ree.es/es/pvpc, 2021 (accessed October 4, 2021).
[68] Observatorio astronómico nacional: Horas de salida y puesta de sol, Instituto Geográfico Nacional de España, 2021 (accessed October 4, 2021), https://astronomia.ign.es/hora-salidas-y-puestas-de-sol.
[69] P. Charbonneau, B. Knapp, PIKAIA. High Altitude Observatory, National Center for Atmospheric Research (NCAR), 2021 (accessed October 4, 2021), http://www.hao.ucar.edu/modeling/pikaia/pikaia.php#sec1.
[70] C. Song, P. Wang, H.A. Makse, A phase diagram for jammed matter, Nature 453 (2008) 629–632, https://doi.org/10.1038/nature06981.